12-2018

Combining Atomic Force Microscopy and Shear-force Acoustic Near-field Microscopy to Characterize Confined Mesoscopic Fluids

Monte Allen Kozell
Portland State University

Theodore Brockman
Portland State University

Andres H. La Rosa
Portland State University, andres@pdx.edu

Citation Details

Kozell, M., Brockman, T., & La Rosa, A. H. (2018, December). Combining atomic force microscopy and shear-force acoustic near-field microscopy to characterize confined mesoscopic fluids. In Journal of Physics: Conference Series (Vol. 1143, No. 1, p. 012015). IOP Publishing.

Combining atomic force microscopy and shear-force acoustic near-field microscopy to characterize confined mesoscopic fluids

IOP Conf. Series: Journal of Physics: Conf. Series **1143** (2018) 012015 doi:10.1088/1742-6596/1143/1/012015

Combining atomic force microscopy and shear-force acoustic near-field microscopy to characterize confined mesoscopic fluids

Monte Kozell[1,2], **Theodore Brockman**[1] **and Andres H La Rosa**[1]

[1] Physics Department, Portland State University, Physics Department, Portland, OR, USA
[2] Lam Research, Tualatin, OR, USA

E-mail: montekozell@gmail.com, andres@pdx.edu

Abstract. An atomic force microscopy (AFM) cantilever is integrated into to a quartz tuning fork (QTF) to probe the viscoelastic properties of mesoscopic fluid layers confined between two solid surfaces under shear. Two procedures to fabricate the AFM/QTF probe are described herein. In the first, a nano-manipulator is used to transport a commercially available afm cantilever from its chip holder to the edge of a QTF tine. In the second, an afm cantilever is fabricated at the edge of the QTF tine itself. In both cases we exploit the capabilities of a dual-beam system (focused ion beam/scanning electron microscope), equipped with Omni-Probe nano-manipulator and a Gas Injection System (GIS). The new device improves the ability of shear-force acoustic near-field microscopy (SANM) to monitor the constraining normal and damping shear forces exerted by the solid boundaries, concurrently with the acoustic emission from the trapped fluid.

1. Introduction

Shear-force Acoustic Near-field Microscopy (SANM) was recently introduced as a metrology tool to characterize the dynamic behavior of mesoscopic fluids trapped between two solid boundaries under relative shear motion. SANM measurements emphasize, in particular, the near-field detection of acoustic waves emitted from a trapped mesoscopic fluid[1,2], which offers complementary information to the simultaneously acquired shear-force also intervening in the probe-fluids interactions. This scenario is akin to interfacial friction phenomena (wear-less friction[3]) where the dissipation of energy is attributed to inelastic interactions between the solid boundaries and the confined fluid layer (with no solid-probe and solid-substrate contact.) The added acoustic detection capability brought by the new SANM technique allows contrasting the acoustic signal emitted by the fluid with the information obtained from the simultaneously acquired damping shear-force acting on the probe, which illustrates the improved metrology capabilities offered by SANM. Still, at its current state of development, this new technique lacks the ability to measure the normal force component of the solid-fluid interactions. This shortcoming is addressed herein.

In SANM, a tapered stylus (size of the apex radius of curvature typically tens of nanometer) is adhered to a quartz tuning fork (QTF), which is electrically driven at resonance frequency condition (~ 10 nm amplitude.) The probe is then allowed to interact with a substrate. The lateral oscillation amplitude of the tuning fork is routinely used as a feedback signal to control the probe-sample distance[4,5]. A benefit of the shear motion operation (probe oscillating parallel to the surface boundaries) is that the tip is kept at a fixed height above the sample surface, thus removing a direct tapping (*i.e.* intermittent contact) of the probe

against the sample. Removing such a direct mechanical interaction extends the probe lifespan and reduces sample damage. However, one issue in the SANM field is the inconclusive knowledge of the absolute value of the probe-substrate separation distance, *i.e*. there is an uncertainty about the exact location of the substrate [6]. This causes ambiguity when interpreting the probe-fluid interaction mechanisms as a function of probe-sample separation distance. For the particular cases where the probe and substrate are electrically conductive, the exact location of the substrate can be established by monitoring the onset of the tunneling current across the probe-substrate gap. An exponentially increasing current is initiated when a biased probe comes into mechanical contact with the surface. But the method is applicable only to conductive samples.

Atomic Force Microscopy, by contrast, allows a direct vertical spatial mapping of the normal force components of the interaction as a function of probe-sample separation distance. The AFM consists of a beam cantilever that has a pyramid shape apex. AFMs typically operates by reflecting a laser off the cantilever and onto a position-sensitive photodiode (pspd). As the cantilever gets closer to the substrate, the intervening normal forces bend the cantilever, which results in a deflection of the laser spot centered on the pspd. The recorded normal force traces typically display two well-defined interactions regions. In the first region one can interpret the probe interacting with a mesoscopic water layer; in the second, the probe certainly undergoes a direct mechanical contact given linear response tracked by the pspd[7].

In the present work, we incorporate the functionality of an afm beam cantilever into the SANM. We focus in the description of an AFM/QTF probe fabrication method. In subsequent work we plan to use this system to obtain approach curves that monitor normal force, lateral shear force, lateral displacement and the acoustic amplitude to spatially map probe-sample interactions as a function of separation distance.

2. Probe Device Fabrication

A commercial non-contact (NanoSensor, NCH-W) afm cantilever was directly adhered onto the tine of a commercial 32,768 Hz QTF (Abracon, AB26TRQ-32.768KHz-T). A XE-120 PSIA (Park) AFM system was used for this experiment. The QTF was first adhered (using cyanoacrylate) to a commercial stainless steel mount in such a way that the tines oscillate parallel to the sample surface.

2.1 Method 1: Attachment of an AFM Cantilever to a QTF

A dual-beam FIB-SEM FEI Helios 400s, equipped with Omni-Probe nanomanipulator and gas injection system (GIS), is used to adhere an afm cantilever to the QTF tine. GIS gases comprising platinum and carbon are used. As starting material, a commercial afm cantilever comes already attached to a metal chip holder (for easy handling) as shown in Fig. 1.

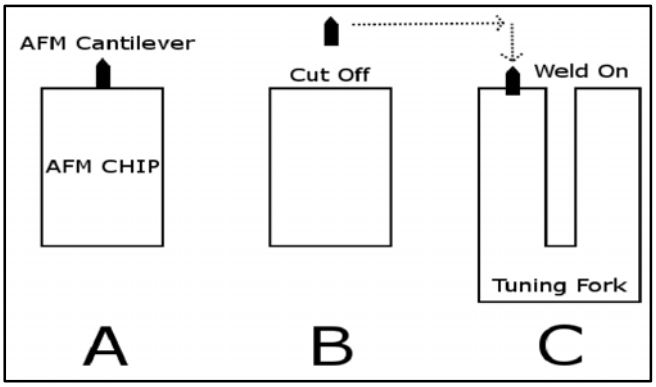

Figure 1: Schematic procedure to prepare an AFM/QTF probe**. (A)** Unmodified afm cantilever attached to a metal chip, as received from the manufacturer. **(B)** Afm cantilever cut free from the chip. **(C)** Cantilever afm welded onto the tuning fork tine.

As a first step, the afm chip and the QTF are mounted flat inside the FIB-SEM system. The Omni-Probe nanomanipulator is lowered to a height of approximately 1 μm above the cantilever surface (Fig. 2A and

2B), followed by the insertion of the platinum GIS needle into the chamber (Fig. 2C.) In the presence of a gas source inserted through the GIS needle, a gallium ion beam (30 kV and 300 pA) allows welding the cantilever to the Omni-Probe (Fig. 2D). In this process, while the gas is injected into the chamber, the ion beam rastered over a selected area generates secondary electrons, which subsequently break down the precursor gas (platinum or carbon) that ends up deposited onto the surface[8].

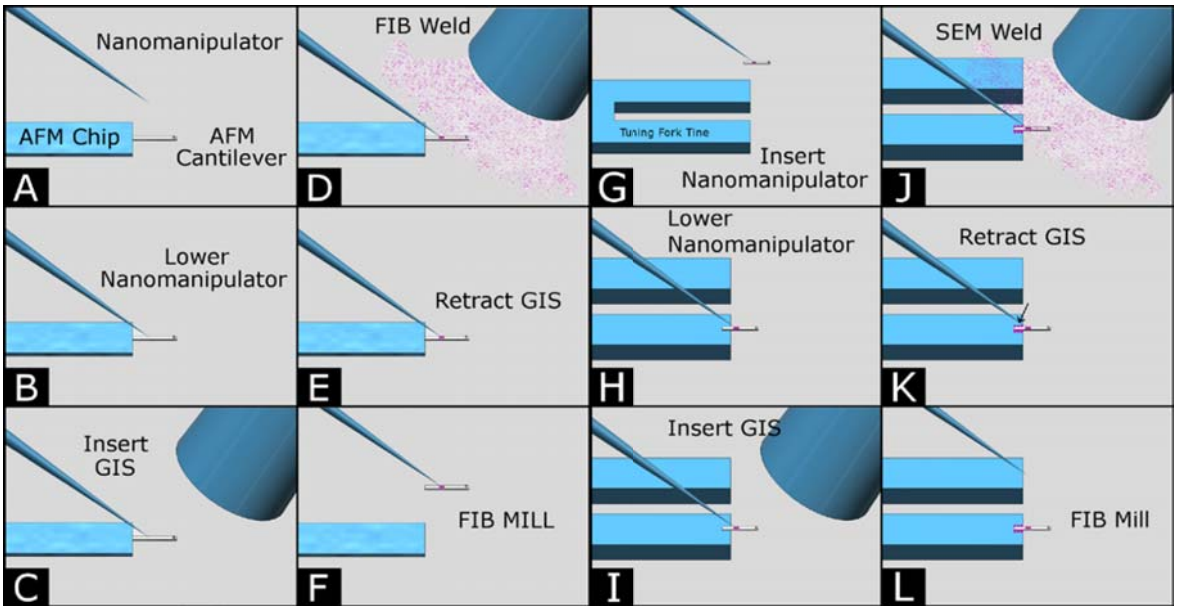

Figure 2: Sequential procedure of extraction of an afm cantilever and its attachment to the nanomanipulator (A to F). **(A)** Omniprobe nanomanipulator is inserted. **(B)** Nanomanipulator placed approximately 1μm above the afm cantilever. **(C)** Insertion of the platinum gas injection needle. **(D)** Platinum gas injected into the chamber while the ion beam weld is in pattern mode; this procedure welds the nanomanipulator to the afm cantilever. **(E)** Cantilever welded to the nanomanipulator. **(F)** FIB milling cuts the afm cantilever free from the chip. The nanomanipulator is raised above the sample and retracted. **Sequential procedure of attachment of the afm probe to a QTF-tine (H to L)**: **(G)** Nanomanipulator inserted. **(H)** The nanomanipulator is placed at approximately 1 μm above the QTF tine. **(I)** Platinum gas injection needle inserted into the chamber. **(J)** Platinum gas is injected into the chamber while the electron beam weld is in patterning mode, which welds the afm cantilever to the QTF tine. Several platinum welds points insure a secure attachment. **(K)** Electron beam welding completed. Electron beam deposition was used instead of ion deposition due to irregular gas flow caused by the large afm cantilever geometry impeding platinum gas flow. Ion deposition attempts resulted in milling instead of deposition. **(L)** Once welded, the nanomanipulator is FIB cut free, then lifted and retracted.

The welding is performed at the center of the cantilever to thus reduce the probability that a 125 μm long-arm afm cantilever collides with other internal SEM chamber components. The cantilever is then cut free near the afm chip-cantilever interface using the Ga-ion beam operated at 30 kV and 2.5 nA (fig. 2E). Subsequently, the GIS needle is retracted from the chamber. With the afm cantilever adhered to the Omni-Probe, the probe is raised to a safe height of approximately 200 μm above the afm chip and then retracted for safely moving the stage positions (Fig. 2F).

The FIB-SEM sample stage is positioned to work over to QTF tine. The Omni-Probe needle is lowered to a height of approximately 1μm above the tuning fork tine (Fig. 2G and 2H). The platinum GIS needle is inserted into the chamber (Fig. 2I). An SEM beam (10kv, 3.2nA) is used to weld the afm cantilever onto the end of the tuning fork tine (Fig. 2J). The Omni-Probe needle is cut free using the Ga-ion beam, 30 kV, 2.5 nA (Fig. 2K). Finally, the platinum GIS is retracted and the Omni-Probe raised to a height of approximately 200 μm and retracted (Fig. 2L).

Fig. 3 shows SEM images of the resulting AFM/QTF probe. Fig. 3A shows the actual tuning fork tines with an afm cantilever attached with electron beam platinum welds. Fig. 3B is a higher magnification image of the afm cantilever. Note the platinum weld at the center of the cantilever, which was used to temporarily adhere it to the nanomanipulator. The afm tip is at the top side.

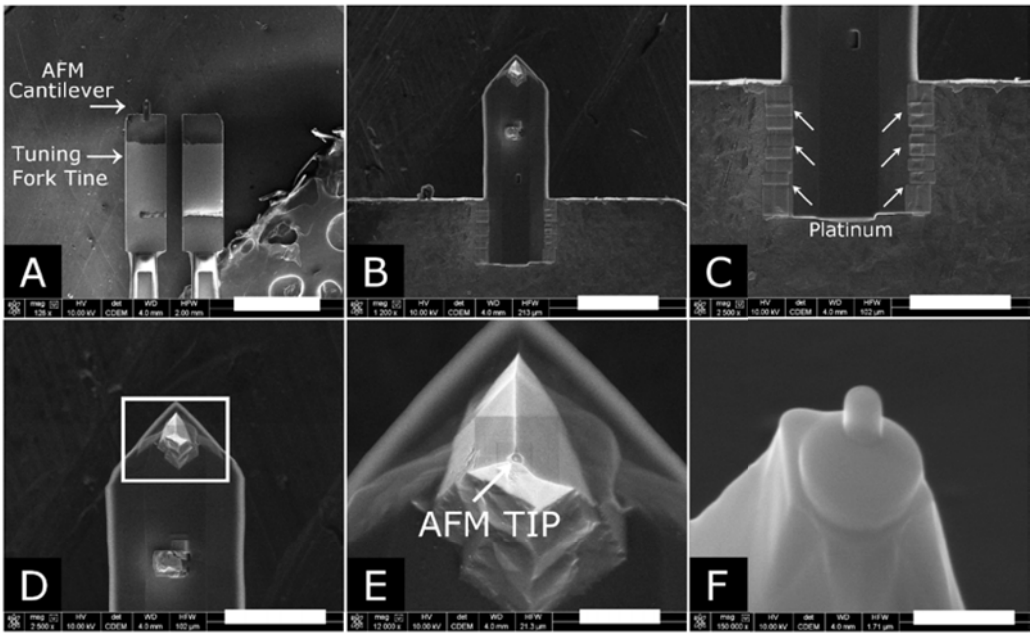

Figure 3: (A) QTF with an afm cantilever attached (via electron beam platinum welding) to one of its tines. Scale bar is 500 μm. **(B)** Image of the afm cantilever. Note at the center the platinum weld that was used to temporarily adhere the cantilever to the nanomanipulator. The afm tip is located near the edge. Scale bar 50 μm **(C)** Platinum welds adhering the cantilever to the tuning fork tine. Scale bar 30 erμm **(D)** High magnification image of the tip. Scale bar 30 μm **(E)** Carbon tip pyramid fabricated at the apex via Ga ion beam deposition. Scale bar 5 μm **(F)** Tilted image of the IBD carbon tip. Scale bar 500 nm.

Fig. 3C shows the platinum welds securing the attachment of the cantilever to the QTF tine. Fig. 3D is a higher magnification image of the cantilever apex. Fig. 3E is a top down (zero tilt) image of the pyramid structure of the afm, with a Ga ion beam deposited carbon tip. Fig. 3F shows a 52 degree tilted image of the ion beam deposited (IBD) carbon tip of base of radius 500 nm, tip height of 250 nm, and tip radius ~110 nm. By using a FIB mill/deposition method, old tips that have been damaged can simply be FIB milled away and a new carbon tip can be grown. Other materials can be used for tip growth, such as platinum, tungsten or insulator SiO_2. Electron beam deposited carbon tips[9] and ion beam deposited tips[10] have been shown

to be effective for imaging purposes. IBD carbon probes have 70 Gpa shear modulus[11], 9-10 Gpa hardness, and 123-130 GPa Young's modulus[10].

2.2. Method 2: Focused Ion Beam Milled Cantilever Fabrication

We have also explored an alternative fabrication method, where a beam cantilever is built in at the corner of QTF tine. Fig. 4 shows the overall strategy. First, the QTF tine is properly FIB carved to create a thinner section; a subsequent ion mill of a groove results in the formation of a flat rectangular cantilever. A small area of one side of the cantilever is coated with a metallic pad (to increase its light reflectivity). On the other side, a pyramid shape tip is fabricated. The fabrication process is described in more detailed next.

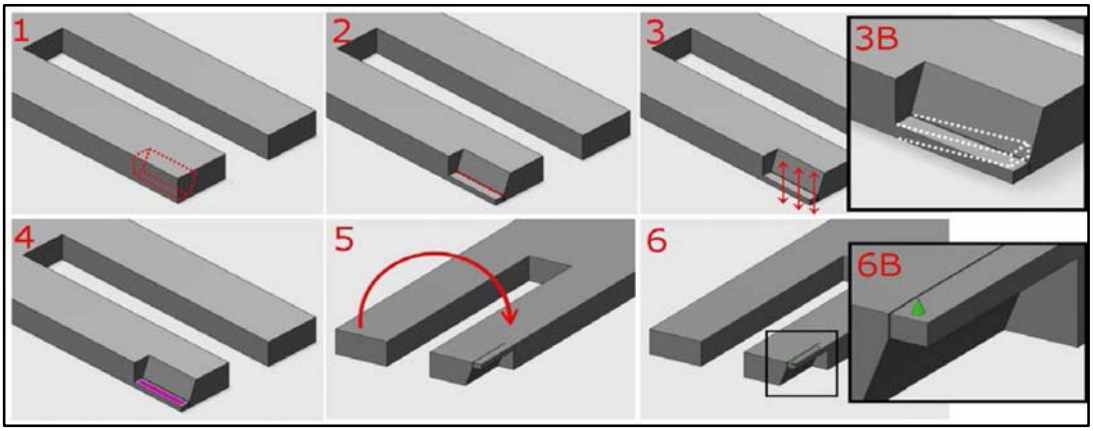

Figure 4 Sequence of the fabrication procedure of a cantilever built-in into a QTF-tine using a focused ion beam (FIB). **Image 1:** Volume section (red dots) of a QTF selected for ion beam milling. **Image 2:** QTF tine post FIB milling. Red dots illustrate another milled region that allows the cantilever the ability to flex in the vertical direction. **Image 3:** Cantilever flexing vertically. **Image 3B** Cantilever flexing range motion. **Image 4** Cantilever after ion-beam-deposited (IBD) platinum pad (purple color) deposited on the top of the cantilever, for improving laser reflection. **Image 5** Cantilever flipped over so a carbon probe can be fabricated. **Image 6** and **6B** illustrates the IBD probe (green color) onto the end of the cantilever.

We fabricate a pyramidal-shape platinum base followed by carbon tip at the apex. For constructing the base, a gallium ion beam and an in situ platinum gas injection system were used to deposit platinum onto the QTF tine. As a precursor gas we used (methylcyclopentadienyl) trimethyl platinum, $C_9H_{16}Pt$ (FEI, Helios 400s User Manual.) The platinum base (8x8 μm^2) was built-up with sequential deposition of platinum layers of reduced width reach time (current density of 2-6 pA/μm^2), as schematically illustrated in figures 5 A-C. After the deposition of 13 layers, the width of the apex was 1.5 μm. Then, carbon was deposited via gallium ion deposition (at current densities of 1-10 pA/μm^2); see figures 5 D-F. IBD carbon deposition occurs at a faster rate than platinum, hence the increased taper slope of the pyramid tip [12]. The final tip was deposited under spot mode (where the raster scanning of the FIB beam is disabled) and its growth occurs rapidly (often taking less than 30 sec.) The total height (base plus tip) is ~5 μm.

Attempts to build an afm pyramid tip directly out of carbon deposition on the QTF proved to be difficult. The reason is basically due to electron charge that builds up when performing electron beam deposition on insulating materials (Quartz resistivity between 10^5 to 10^{18} Ωm)[13]. Charge buildup results in a repulsive electric field developing on the tuning fork tine, causing electron beam induced tip growth to be skewed in

a lateral direction. Proper grounding of the tuning fork electrodes allowed charge build-up to be reduced, but not always eliminated. As an alternative, it was decided to produce Gallium ion deposited carbon tips for experimental use. Since gallium ions are 127,000 times more massive than electrons (Gallium 69.723 u, Electron 5.485×10^{-4} u, unified atomic mass unit), charge build-up has a lesser deflection effect on gallium ion beam path. In addition, the positive gallium ion are attracted to surfaces with built-up electron charge, and has an effect to neutralize the substrate. Limited by the resolution of the ion beam, tip radius of ~100 nm were reliably produced. The table 5 below shows the deposition parameters used for the final carbon tip fabrication.

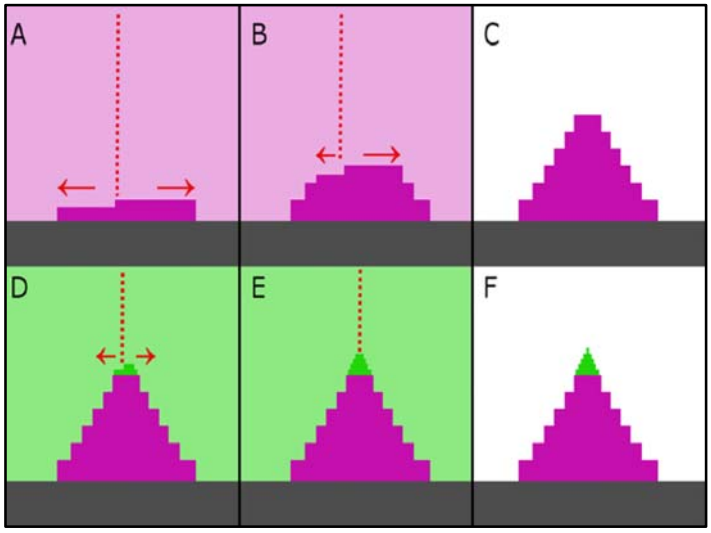

Figure 5: Schematic procedure to fabricate a pyramidal tip near the edge of a beam cantilever. The probe-base is fabricated by sequentially depositing rectangular patterns of IBD platinum as shown in **images A-C**. The ion beam is rastered while platinum gas is injected into the chamber. **Images D-F** illustrates the sequential pattern deposition of the IBD carbon probe tip. The ion beam is rastered while a carbon gas is injected into the chamber. **Image F** displays the final deposition of the probe apex; no FIB rastering was used to minimize probe radius.

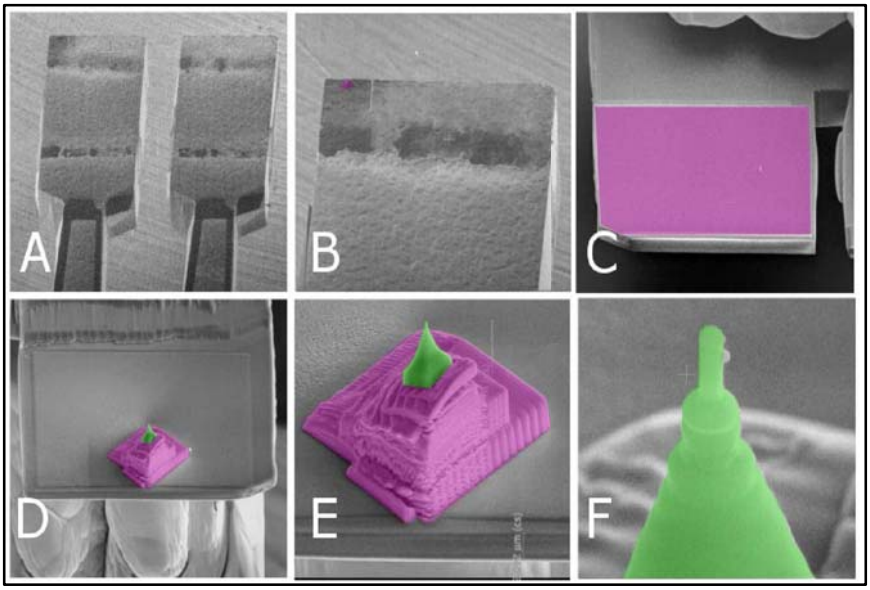

Figure 6. SEM images (with false colors to differentiate materials.) Horizontal field width (HFW) stands for image width. **(A)** QTF lower region; HFW=1.28 mm. **(B)** QTF bottom edge; HFW=320 µm. **(C)** Gallium-ion beam platinum pad (purple) deposited on top of cantilever; HFW=60 µm. **(D)-(E)** First iteration of a Ga-IBD deposited platinum base (purple) with carbon tip (green). HFW=60 µm and 19.5 µm respectively. **(F)** Ga-IBD carbon tip with radius of 100 nm; HFW=2.0 µm.

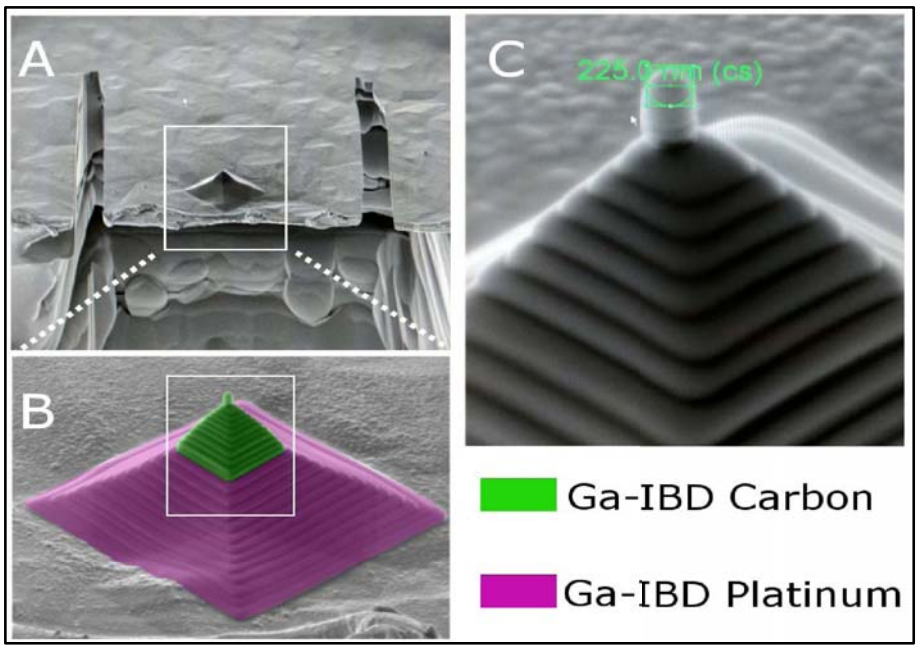

Figure 7. Refined fabrication iteration of a platinum-base and a carbon-tip. **(A)** FIB milled cantilever and platinum pyramid base fabricated with Ga IBD deposition. HFW= 73.1 µm. **(B)** Higher magnification with false colors of the platinum base (purple) and the carbon-tip (green); HFW=17.1µm. **(C)** Carbon tip of 112 nm radius; HFW = 2.0 µm.

2.3 Estimation of the probe's spring constants

The length, width, thickness and tip height of the cantilever determine its spring constants in the normal, lateral, and torsional directions. Table 1 shows pertinent equations showing the relation between spring constants and cantilever dimensions. Table 2 gives the dimensions of FIB milled cantilevers; 76.5 µm in length, 35 µm width, and 5 µm thickness. The estimated cantilever spring constant in the normal dimension was approximately 196 N/m, much stiffer than typical tapping mode cantilevers commercially available (20-70 N/m). This will allow the AFM/QTF cantilever to reliably probe closer to the sample surface before undergoing a jump-to-contact. The lateral spring constant is estimated to be 12,000 N/m, while the torsional spring constant is 23,800 N/m. Both torsional and lateral spring constants are sufficiently large that displacement in either dimension will be small compared to normal displacement. Table 3 shows the material properties used for determining the spring constants and contains material properties of the crystal quartz tuning fork (SiO_2), and the ion beam deposited carbon used to fabricate the tip. Table 4 summarizes the estimated spring constants of the fabricated cantilever.

Table 1: Equations for Spring Constants	
Normal Force Constant K_{ver}	$K_{ver}=w*E/4*(t/l)^3$
Lateral Force Constant K_{lat}	$K_{lat}=t*E/4*(w/l)^3$
Torsional Force Constant K_{tor}	$K_{tor}=w*(G/3)*(t^3/l)/(H+t/2)^2$
t=thickness, w=width, l=length, H = Tip Height; Source [14]	

Table 2: FIB Milled Cantilever Dimensions				
Length (l)	Width (w)	Thickness (t)	Tip Height (H)	Tip Radius (R)
76.5 µm	35 µm	5 µm	5.8 µm	110 nm

Table 3: Material properties		
Quartz Tuning Fork (SiO_2)	Young's Modulus E(Perp) & E(Para) Shear Modulus G	E(perp) = 78.7 GPa [15] E(para) = 98.2 GPa G = 31.14 GPa [16]
IBD Carbon (Tip material)	Shear Modulus G	G = 70 GPa [11]

Table 4: FIB Milled Cantilever Spring Constants		
K_{ver}	K_{lat}	K_{tor}
196 N/m	12,000 N/m	23,800 N/m

Table 5: Summary of Ion-beam Tip Deposition Parameters			
Deposition Parameters	Accelerating Voltage	Beam Current	Deposition time
IBD Carbon	30 kV	13 pA	15 sec

3. Conclusions

Two procedures for fabricating an AFM type pyramid at the edge of a quartz tuning fork (QTF) were successfully implemented. The project pursued obtaining a robust probe, less susceptible to "jump to contact" instability (characteristic of commercially available typical afm cantilevers), still sensitive enough to measure normal forces. The "jump to contact" on regular fragile cantilevers is caused by the coalescence of a water meniscus that occurs when the pyramid probe is placed near another substrate at ambient conditions. The latter is detrimental to a metrology system. The probes fabricated here are one order of magnitude stronger. In combination with a QTF, the pyramid tip can also be driven into lateral oscillations, which enable the trapped fluid layer/meniscus to emit acoustic waves. The ability to detect such near-field acoustic waves is a peculiar capability in Shear-force Acoustic Near-field Microscopy (SANM). The ability to measure normal forces, lateral forces, and acoustic emission from solid/fluid interfaces elevates the status of SANM as a nanometrology system.

Acknowledgements

This work was supported in part by Lam Research Corporation, CA USA.

Bibliography

[1] La Rosa A H, Cui X, McCollum J, Li N and Nordstrom R 2005 *Rev. Sci. Instrum.* **76** 093707
[2] Fernandez R, Wang X and La Rosa A H 2011 *Proceedings of the Nanotechnology* (*IEEE-NANO*) *11th IEEE International Conference* 903
[3] Karrai K, Tiemann I 2000 *Phys Rev B: Condens Matter Mater Phys*. **62** 13174
[4] Bharat Bhushan 2012 NANOSCIENCE and NANOTECHNOLOGY Scanning Probe Microscopy in Nanoscience and Nanotechnology, Volume 3 (Springer).
[5] Ruiter A G, van der Werf K O, Veerman J A, Garcia-Parajo M F, Rensen W H, van Hulst N F 1998 *Ultramicroscopy* **71** 149
[6] Cui X, La Rosa A H 2005 *Appl. Phys. Lett.* **87** 231907
[7] Cappella B, Dietler G 1999 *Surf Sci Rep.* 1**34**(1-3):1–104
[8] Lipp S, Frey L, Lehrer C, Demm E, Pauthner S and Ryssel H 1996 *Microelectron. Reliab.* **36** 1779
[9] Schiffmann K I 1993 *Nanotechnology* **4** 163
[10] Lemoine P, Roy S S, Quinn J P, Maguire P D and McLaughlin J A D 2007 *Appl. Phys. A: Mater. Sci. Process* **86** 451
[11] Nakamatsu K, Nagase M, Namatsu H and Matsui S 2005 *Jpn. J. Appl. Phys.* **44** L1228
[12] Yao N Focused Ion Beam Systems: Basics and Applications (Cambridge University Press).
[13] Jair H and Nowick A S 1982 *Journal of Applied Physics* **53** 477
[14] Eaton P, West P 2010 Atomic Force Microscopy (Oxford University Press)
[15] Castellanos-Gomez A, Agraït N, Rubio-Bollinger G. 2009 *Nanotechnology* **20** 215502
[16] Götze J 2009 *Mineralogical Magazine* **73** 645